Langmuir

Article

pubs.acs.org/Langmuir

Development of a Highly Active Electrocatalyst via Ultrafine Pd Nanoparticles Dispersed on Pristine Graphene

Jian Zhao,*[,†,‡,§] Zhensheng Liu,[†] Hongqi Li,[†] Wenbin Hu,[†] Changzhi Zhao,[†] Peng Zhao,*[,‡,§] and Donglu Shi[§]

[†]Key Laboratory of Rubber-Plastics Ministry of Education/Shandong Provincial Key Laboratory of Rubber-Plastics, Qingdao University of Science and Technology, No. 53 Zhengzhou Road, Qingdao 266042, China

[‡]East Hospital, Tongji University School of Medicine, Shanghai 200120, P. R. China

[§]The Materials Science and Engineering Program, Dept. of Mechanical and Materials Engineering, College of Engineering and Applied Science, University of Cincinnati, Cincinnati, Ohio 45221, United States

Supporting Information

ABSTRACT: A unique synthesis was developed to immobilize Pd nanoparticles on pristine graphene (PG) sheets via a facile supercritical carbon dioxide route. Pristine graphene was obtained by sonication-assisted exfoliation of graphite in an organic solvent. Finely dispersed worm-like Pd nanoparticles are homogeneously deposited on the hydrophobic graphene surfaces. The combination of pristine graphene sheets and well-dispersed Pd nanoparticles provided large electrochemically active surface areas (ECSA) for both direct formic acid fuel cell (DFAFC) and methanol fuel cell (DMFC). The ECSA values are more than twice as large as those of reduced graphene oxide and carbon nanotube based counterparts or six times those of conventional XC-72 carbon black. Significant enhancements were also observed in the electrocatalytic activity and stability measurements. The excellent electrochemical property of Pd/PG is attributable to the well-preserved graphene structure that ensures electrical conductivity and stability of the composite. Its large surface area also allows for the deposition of small size and high dispersion of the Pd nanoparticles. This straightforward synthesis offers a new pathway for developing highly active electrocatalysts based on pristine graphene with fully optimized properties.

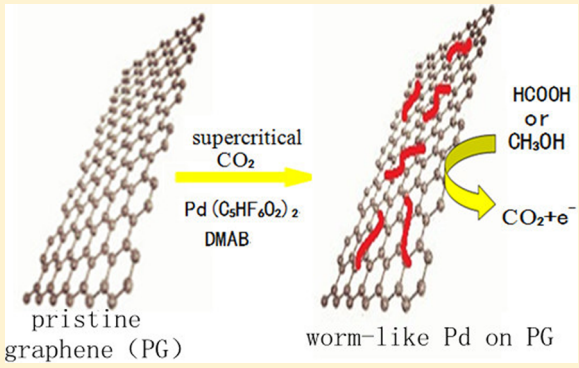

1. INTRODUCTION

Recently, direct methanol fuel cells (DMFCs) and direct formic acid fuel cells (DFAFCs) have attracted appreciable attention for their high efficiency of energy conversion, low operating temperature, reduced pollutant emission, and easy management.[1−3] As is well known, platinum has been the primary catalyst in both DMFC and DFAFC. However, with platinum as an anode catalyst, the surface is usually heavily poisoned by strong adsorption of CO intermediates, resulting in the lowering of catalytic performance. The high cost of platinum is also a drawback for commercial applications. In an effort to reduce the cost and improve the activity of catalysts, attention has been shifted to non-Pt materials. Recent results have identified Pd as a suitable alternative for its higher abundance, lower cost, and greater resistance to CO.[4,5] Nevertheless, the commercialization of the fuel cell technology is still hindered by the low utilization efficiency and poor catalytic performance of Pd.[6,7]

The commonly used strategy to address these critical issues is to disperse Pd nanostructures on the surface of the supporting materials.[8] For an ideal substrate, it requires high inertness in extreme conditions. A large surface area is also needed for fine dispersion of catalyst nanoparticles.[9] Furthermore, the supporting materials must be highly conductive and have low cost. In order to achieve the requirements for high performance, the interfaces between metal nanoparticles and the supports also play a crucial role. Pd particles have been loaded on various carbon substrates including carbon black (CB, e.g., Vulcan XC 72),[10] carbon nanofibers (CNFs),[11] and carbon nanotubes (CNTs)[12,13] to improve the activity and stability of the fuel cells. Among carbon-based substrates, graphene exhibits a unique 2-D honeycomb carbon structure with a large surface area and high electrical conductivity.[14,15] These unique structural and physical attributes ideally satisfy the requirements for a stable catalyst structure. The combination of graphene sheets and Pd nanoparticles has shown promising characteristics for the next-generation electrocatalysts.[16,17]

Currently, the methods of hybridizing graphene with metallic Pd are dominated by those of using graphene oxide (G-O) sheets as a raw material or precursor of graphene sheets.[16−22]

Received: December 19, 2014
Revised: January 31, 2015
Published: February 18, 2015

DOI: 10.1021/la5049425
Langmuir 2015, 31, 2576−2583

Abundant oxygen-containing functionalities on graphene oxide allow for its full exfoliation in several solvents and provide binding sites for the metallic nanoparticles. However, the conductivity of graphene may suffer considerably by excessive oxygen-containing functional groups due to disruption of the sp^2-hybridized carbon network. Previous studies have shown that it is not likely to restore the intrinsic electronic conductivity even by removal of the functional groups.[23,24] The high density of graphene surface defects makes the hybrids unstable under harsh electrocatalytic environment. Hence, the development of novel Pd−graphene catalysts with low-density-defect graphene such as pristine graphene is highly desirable for property improvements.

Efficient immobilization of metallic nanoparticles onto pristine graphene has proven difficult. Few studies have been reported on the decoration of metallic nanoparticles on the hydrophobic surfaces of pristine graphene. Stabilizers or surfactants were utilized to enhance the compatibility of graphene in solvents and stabilize metal nanoparticles on graphene surface.[25,26] Unfortunately, the surfactant molecules may strongly absorb on the surface of metal nanopartilces and greatly decrease the performance of the catalysts.[27] We previously investigated Pt- or Pt-based Ru alloy on thermally reduced graphene via a supercritical route.[28,29] A high density of defects was found on the graphene surfaces during thermal expansion of GO, which served as nucleation sites for the metal nanoparticles. However, these defects would adversely influence the electrocatalytic properties.

Direct deposition of Pd nanoparticles on pristine graphene was successfully achieved in this study by a modified supercritical CO_2 route. The supercritical fluids exhibited a gas-like diffusion rate and near-zero surface tension. Ultrafine Pd metallic nanoparticles were directly deposited on pristine graphene sheets under the assistance of the supercritical fluid. H_2 was replaced with dimethyl amine borane as a reducing agent, which greatly simplified experimental procedure. This replacement also significantly lowered the synthesis temperature (50 °C) for metal reduction.[24,30] The highly graphitized surface was finely decorated by the Pd nanoparticles upon one-pot supercritical treatment.

Besides pristine graphene, reduced graphene oxide (RGO), carbon nanotubes (CNT), and carbon black (Vulcan XC-72) were investigated as support materials in the development of Pd catalysts for formic acid and methanol electro-oxidation. The Pd/PG catalyst exhibits high electrical conductivity and promoted activity and stability for formic acid and methanol oxidation, far preceding Pd/RGO, Pd/CNT, and Pd/XC-72 hybrids.

2. EXPERIMENTAL SECTION

2.1. Materials. Multiwalled carbon nanotubes (CNTs) were obtained from Shenzhen NTP. Co. Ltd. (Shenzhen, China) (with a range of diameter 20−40 nm, length ≤ 2 μm, purity ≥ 99%, specific BET surface area of 70−150 m^2/g). Carbon black (Vulcan XC-72) with a specific BET surface area of 250 m^2/g was purchased from Cabot. Natural Graphite flakes (purity 99.99%, particle size 40 μm) were obtained from Qingdao Ruisheng Graphite Co. Ltd. Dimethyl amineborane (DMAB) was purchased from Aldrich. Palladium(II) hexafluoroacetylacetonate was obtained from Alfa Aesar.

2.2. Preparation of Graphite Oxide (GO). Graphite oxide was prepared from graphite using the modified Hummers method.[31,32] Typically, 3.5 g of $NaNO_3$ and 5.0 g of graphite powder were put into 250 mL of concentrated H_2SO_4 under magnetic stirring in an ice bath. Afterward, 25 g of $KMnO_4$ was added over a period of 1 h, and the temperature of the mixture was kept below 15 °C. The mixture was then stirred at 35 °C for 96 h. A 5 wt % amount of H_2SO_4 aqueous solution was added, and the temperature was maintained at 96 °C for 3 h. Afterward, the temperature was decreased to 60 °C, and a 30 wt % H_2O_2 solution (15 mL) was added to terminate the reaction, followed by stirring for 2 h at 35 °C. The mixture was filtered and washed with 0.5 wt % H_2O_2/3 wt % H_2SO_4 solution, 5 wt % HCl solution, and a large amount of distilled water. Finally, the product was vacuum dried at 50 °C for 72 h to obtain GO.

2.3. Synthesis of Pristine Graphene. A dispersion of pristine graphene in NMP (150 mL) was prepared by ultrasonic tip-sonication treatment of graphite flakes (1.0 g) at 150 W for 72 h.[33] The suspension was then subjected to centrifugation at 600 rpm for 3 h. The top 70% of the dispersion was then collected, followed by filtering through a nylon membrane and washing with methanol. The product was vacuum dried at 60 °C to obtain pristine graphene film.

2.4. Synthesis of Catalysts. Pristine graphene (PG), reduced graphene oxide (RGO), carbon nanotubes (CNT), or carbon black powder (Vulcan XC-72, Cabot) were used as support materials for the catalysts. Typically, pristine graphene (20 mg) was sonicated and dispersed in a mixed solvent of NMP/methanol (6 mL, volume ratio = 2:1) for 1.5 h. Afterward, 25 mg of palladium(II) hexafluoroacetylacetonate and 20 mg of dimethyl amine borane were added. The suspension was put into an autoclave (25 mL). CO_2 was then charged into the reactor and kept at a pressure of 18 MPa and 50 °C. The system was magnetically stirred for 5 h before depressurized. Catalyst product was collected, followed by sonication and washing several times with methanol. The product sample was then dried in vacuum at 60 °C for 24 h. Similarly, carbon nanotubes and carbon black-based composites were prepared under identical conditions. Initially, RGO-supported Pd composites were produced under the same conditions (50 °C) by using GO. Unfortunately, GO could not be sufficiently reduced at low temperature, so that no remarkable electrocatalytic activity was detected. We therefore increased the temperature to 180 °C to fully reduce graphite oxide. It is known that the dispersion state of noble metal particles on RGO could not be affected at this temperature).[34]

2.5. Electrocatalytic Property Measurements. The electrochemical measurements (cyclic voltammogram and chronoamperometry) were made using a three-electrode cell at 25 °C on a CHI660 Electrochemical Workstation. A Pt wire and Ag/AgCl were used as the counter and reference electrodes, respectively. A glass carbon electrode as working electrode was polished with Al_2O_3 paste and washed ultrasonically in Millipore water. The working electrode was cast with *N,N*-dimethylformamide solution (10 μL) containing catalyst (2.5 mg/mL), followed by drying at room temperature. Afterward, the surface of the catalyst layer was covered by 8 μL of 0.05 wt % Nafion solution. Thus, a thin film formed to prevent catalyst from detaching. The working electrode was dried for 5 h before tests. The electrochemical stability and activity of the composites were measured in 0.5 M NaOH with 1 M methanol and 0.5 M H_2SO_4 with 0.5 M HCOOH by CA and CV tests. The electrolyte solutions were stirred constantly and purged with nitrogen gas. All chemicals used were of analytical grade.

SI 1260 impedance/gain-phase analyzer was used to acquire the impedance spectra (frequencies from 100 kHz to 0.01 Hz with amplitude of 5 mV at 0.2 V vs Ag/AgCl). We used ZPlot and ZView software to analyze the obtained impedance data.

2.6. Characterization. The composites were digested with a hot mixure of HNO_3 and HCl (96 °C, 6 h), followed by being maintained at room temperature overnight.[35] Afterward, a HF solution was added. The temperature was increased to 96 °C and maintained for 2 h. To finally obtain metal contents of the composites, the resulting solutions were measured by inductively coupled plasma spectroscopy/optical emission spectroscopy (ICP/OES) (PerkinElmer, Optima 3300XL with AS 91autosampler).

XRD patterns were carried out using a D-MAX 2500/PC equipped with Cu Kα radiation (λ = 0.15418 nm) and operated at 40 kV and 100 mA. XPS analyses were performed using a RBD upgraded PHI-5000C ESCA system (PerkinElmer). The X-ray source was Al Kα radiation with 1486.6 eV. RBD Augerscan 3.21 software (RBD

DOI: 10.1021/la5049425
Langmuir 2015, 31, 2576−2583

Enterprises, USA) was used to perform the data analysis. Raman spectroscopy was conducted on a Renishaw inVia Raman System 1000. The excitation source was Nd:YAG (532 nm). Scanning electron microscopy (SEM) was performed on a JSM-7500F scanning electron microscope with an acceleration voltage of 5 keV. The morphologies and structures of the composites were probed by TEM on a JEOL 2010 instrument which was equipped with an EDS spectrometer.

3. RESULTS AND DISCUSSION

Structural features of the prepared samples were studied by X-ray diffraction (XRD). Figure 1 shows the XRD patterns of

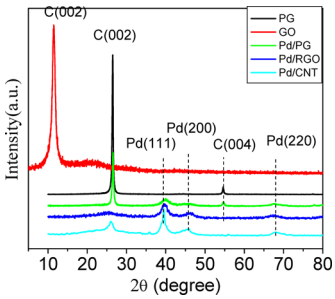

Figure 1. XRD patterns of PG, GO, Pd/PG, Pd/RGO, and Pd/CNT.

dried GO, PG, Pd/CNT, Pd/RGO, and Pd/PG composites. A sharp diffraction peak at 26.5° for dried PG is assigned to the (002) reflection of hexagonal graphite. A minor one at 54.7° corresponds to the (004) plane reflection of crystallized graphite. These data indicate the restacking of the PG sheets upon drying. The graphene characteristic peak of the (002) plane was found to considerably decrease in the Pd/PG composite. This behavior is associated with the aggregation and restacking of graphene sheets being effectively prevented by the attached Pd nanoparticles. The other three peaks in the catalyst at 39.8°, 46.3°, and 67.6° are assigned to the facets (111), (200), and (220) of the face-centered cubic (fcc) Pd lattices, respectively (JCPDS no. 46-1043). This indicates the pure crystalline nature of the Pd nanoparticles. Similar diffraction peaks are found in Pd/CNT.

An intensive peak at $2\theta = 11.1°$ is found in the XRD peak of GO, which arises from the (002) reflection. Upon introduction of the oxygen-containing groups, the average interlayer spacing (0.80 nm) is larger than that of pristine graphite (0.34 nm).[24] In contrast, the (002) peak disappears after the Pd/RGO composite formed, and no striking peaks arising from graphene aggregates are observed. The stacking of the reduced graphene oxide was prevented by the metallic particles while GO was reduced. The other peaks are assigned to metallic Pd.

SEM images (Figure S1, Supporting Information) of both PG and reduced GO (prepared under the same conditions as Pd/RGO) show a layered structure. Figure 2 displays the typical transmission electron microscopy images of the Pd/PG, Pd/RGO, Pd/CNT, and Pd/XC-72 composites. As shown in Figure 2a and 2b, few-layer graphene sheets (very thin) were produced in the preparation processes. The Pd particles in Pd/PG have a unique worm-like shape (Figure 2a), though spherical nanoparticles are occasionally found. These particles are uniformly distributed on the graphene surface with an average size (width) of 3.63 nm in the size range of 1.3−7.7 nm (Figure S2a, Supporting Information). The corresponding SAED pattern shows characteristic Pd diffraction circles (see inset in Figure 2a). The high-quality crystalline feature of graphene is also observed in the diffraction patterns.[37] In

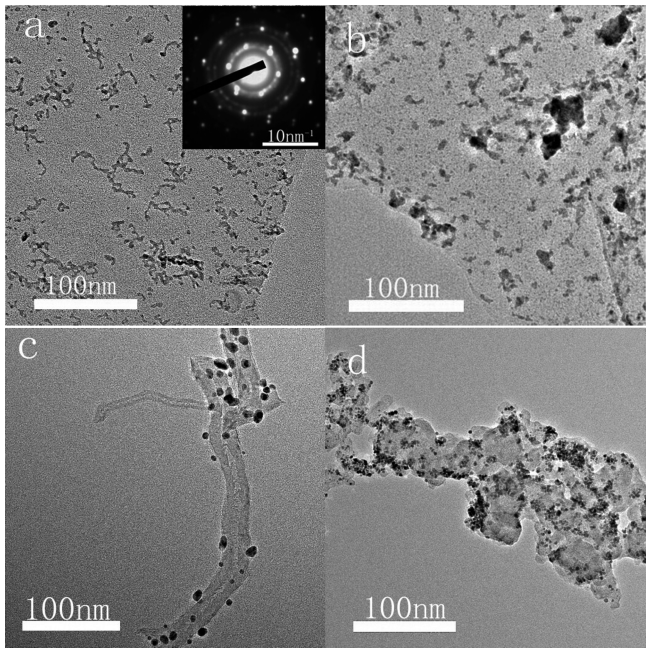

Figure 2. TEM images of Pd/PG with selected area electron diffraction (SAED) pattern as an inset: (a) Pd/PG, (b) Pd/RGO, (c) Pd/CNT, and (d) Pd/XC-72 composites.

contrast, larger and different shaped Pd nanoparticles are randomly distributed on the RGO surface for the Pd/RGO hybrid, as shown in Figure 2b. It is evident that the particle size distribution (1.7−23.8 nm, Figure S2b, Supporting Information) with an average particle size of 8.05 nm is much broader than Pd/PG. Pd/CNT and Pd/XC-72 were prepared under the same experimental conditions as Pd/PG. Spherical Pd nanoparticles are found on Pd/CNT (Figure 2c) and carbon black (Figure 2d). Detailed analysis shows that the average particle size for Pd/CNT and Pd/XC-72 is 7.43 and 5.04 nm in the diameter range from 3.12 to 11.10 nm (Figure S2c, Supporting Information) and from 2.8 to 9.1 nm (Figure S2d, Supporting Information), respectively. High-resolution TEM images of each sample are shown in Figure S3, Supporting Information.

The high-dispersive decoration of Pd nanoparticles on pristine graphene sheets was successful in this study as a result of the supercritical condition which ensured high surface wettability of pristine graphene and effective transfer of the Pd precursors.[9] Recent investigations showed that when nanosized Pd particles are anchored on carbon surfaces, metal Pd species tend to form stable π complexes with unsaturated C−C bonds (C_π). The C_π bonds can act as efficient binding sites for the Pd nanoparticles and play an important role in the generation of Pd−C hybrids.[38] This partly explains the unique worm-like morphology that forms intensive contact with pristine graphene in Pd/PG.

Given the significant functionalization in Pd/RGO, the content of C_π species should be much lower. In addition, although plenty of oxygenated groups on RGO in Pd/RGO are beneficial to the decoration of Pd nanoparticles, an uneven distribution of excessive oxygen-containing groups is not ideal for fine dispersion of the Pd nanoparticles. Furthermore, the graphene conductivity is compromised by an excess of oxygenated groups. The stability of the catalyst is also decreased due to the lower graphitization degree of the carbon

DOI: 10.1021/la5049425
Langmuir 2015, 31, 2576−2583

support. These factors would reduce the electrochemical stability for carbon-supported metal catalysts.

The corresponding energy-dispersive X-ray (EDS) spectra (Figure S4, Supporting Information) show the presence of Pd in Pd/PG Pd/RGO, Pd/CNT, and Pd/XC-72. By inductively coupled plasma (ICP) analysis, the exact content of Pd in the composites is 23.86, 30.75 (higher than other composites because of deoxygenating of GO), 23.01, and 25.39 wt % in Pd/PG, Pd/RGO, Pd/CNT, and Pd/XC-72, respectively.

Raman spectroscopy is a widely used tool for the characterization of carbonaceous materials for conjugated and double carbon−carbon bonds leading to high Raman intensities.[39] Figure 3 shows the Raman spectra of PG, Pd/PG, Pd/RGO, GO, and graphite. The peaks at about 1350, 1580, and 2700 cm^{-1} correspond to the D band, G band, and 2D band of graphene, respectively.[40] The structural defect (sp^3 bonds) is responsible for the D band, while the doubly degenerate E_{2g} mode of graphite give rise to the G band, which is associated with the coplanar vibration of sp^2 atoms in a 2-D hexagonal lattice. The second-order zone boundary phonons result in the 2D band which shifts depending on the number of graphene layers.[41] The I_D to iI_G ratio is small for PG (0.19), indicating an almost perfectly ordered graphitic structure.[42] As compared to the neat graphene sample, the intensity ratios (I_D/iI_G = 0.22) for Pd/PG show minimal increases, an indication of highly crystalline graphene structure which is critical for high electrical conductivity. There is a 2D band at 2707 cm^{-1} in Pd/PG, a structural feature of the few-layer graphene structure in the composites.[39,43]

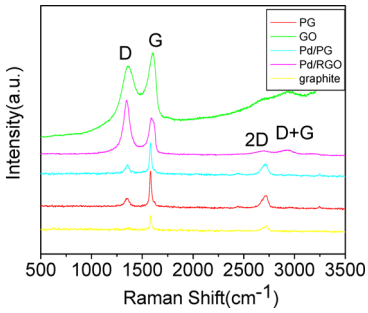

Figure 3. Raman spectra of PG, GO, Pd/PG, Pd/RGO, and graphite.

Comparison of the Raman spectra of graphite and GO shows that both D and G modes intensify and broaden after oxidation. The 2D peak (2725 cm^{-1}) of graphite begins to change after formation of GO (Figure 3). The G bands of Pd/RGO are also found to broaden and upshift as compared to graphite (from 1583 cm^{-1} for graphite to 1591 cm^{-1} for Pd/RGO). The presence of isolated double carbon bonds is responsible for this behavior due to resonance at higher frequencies.[44] The D band at 1346 cm^{-1} is pronounced and associated with structural imperfections originating from the decoration of the epoxide and hydroxyl functional groups on the basal graphene plane.[45] Complete removal of these defects is difficult even using strong reducing reagents.[46,47] The I_D/iI_G ratio varies from 0.85 for GO to 1.40 for Pd/RGO. This increase in D/G intensity ratio is reasonable for reduction could lead to disruption of some carbon−carbon double bonds and the size decrease of the graphene network.[46,47] The overtone (2D) band and combination (D + G) band are also found in the Raman spectrum of the Pd/RGO composite, which are related to the local defects or disorder in the sp^2 phase.[48,49]

Figure 4a, 4b, 4c, and 4d shows the C 1s XPS spectra of PG, GO, Pd/PG, and Pd/RGO, respectively. As a result of GO deoxygenation, a substantial decrease in intensity is found for the −COOH (288.9 eV), −C−O−C− (287.7 eV), and −COH (286.2 eV) functional groups in the C 1s spectrum of Pd/RGO in comparison with the peaks of GO.[50] We also note that the intensities of the oxygenated groups on PG and Pd/PG are much weaker than those on Pd/RGO, indicating a much smaller fraction of oxygenated groups on the graphene sheets. The functional groups on PG might be introduced during purification of natural graphite in its industrial production. The XPS patterns of Pd/PG show significant Pd 3d signals corresponding to the binding energy of Pd (Figure 4e). The relatively lower binding energy set of double peaks (335.6 and 340.9 eV) is due to metallic Pd(0). The double peaks (337.2 and 342.9 eV) can be attributed to the Pd(II) chemical state on PdO or $Pd(OH)_2$.[51] The Pd 3d spectrum of Pd/RGO is similar to that of Pd/PG, as shown in Figure S5, Supporting Information.

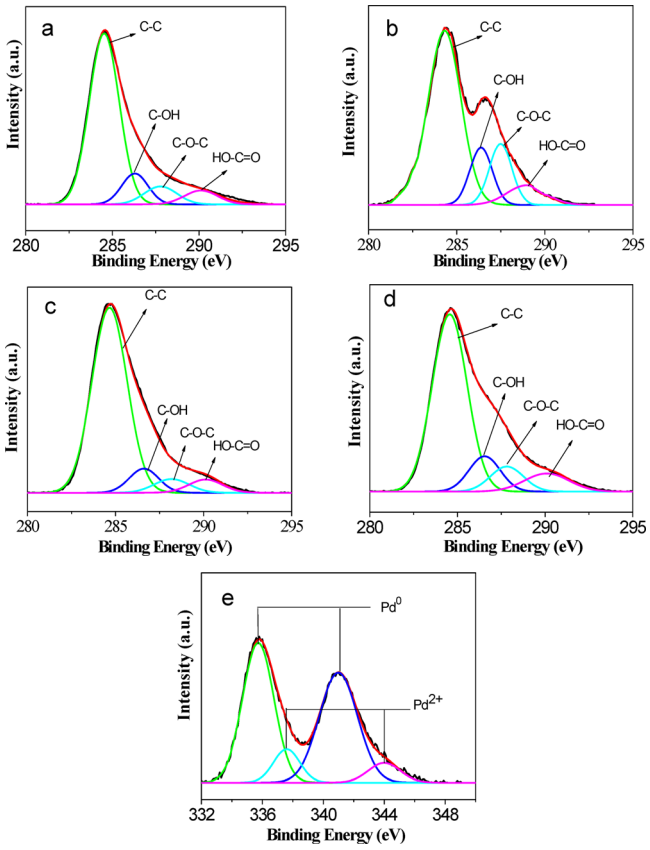

Figure 4. C 1s XPS spectra of PG (a), GO (b), Pd/PG (c), and Pd/RGO (d), and Pd 3d XPS spectrum of Pd/PG (e).

The electrochemically active surface areas (ECSA) of Pd catalysts were estimated by a calculation of the hydrogen desorption area from cyclic voltammograms (CVs) in 0.5 M H_2SO_4 and 0.5 M NaOH solutions. ECSA can provide valuable information on the available active sites of catalysts. It also accounts for the access of a conductive path available to transfer electrons on the electrode surface. Figure 5a shows the CVs of the Pd catalysts in a N_2-saturated solution of 0.5 M H_2SO_4 at 50 mV s^{-1}. In the hydrogen region, the H^+ ions are reduced and the hydrogen atoms are absorbed in the negative-going

DOI: 10.1021/la5049425
Langmuir 2015, 31, 2576−2583

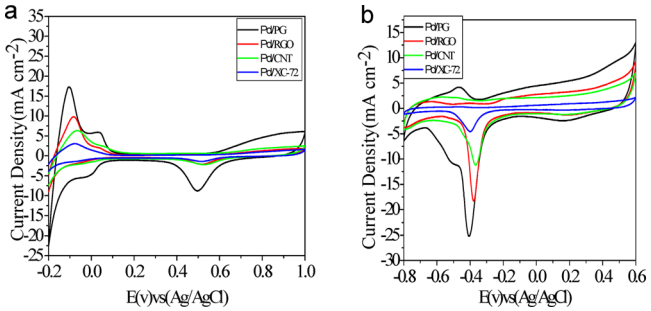

Figure 5. CVs of Pd/PG, Pd/RGO, Pd/CNT, and Pd/XC-72 in 0.5 M H_2SO_4 solution (a) and 0.5 M NaOH solution (b) at 50 mV s^{-1}.

potential scan. In the reverse scan, desorption of the absorbed atoms generates an anodic current. ECSA is estimated by integrating the peak area under the curve that counts for the amount of hydrogen desorbed (Table 1). We find that the

Table 1. Comparison of CV Results for Different Carbon-Supported Samples

	ECSA(m^2/g)		forward peak current (mA/cm^2)		mass activity (mA/mg Pd)	
electrode	DFAFC	DMFC	DFAFC	DMFC	DFAFC	DMFC
Pd/PG	103.8	115.0	84.7	66.9	1045.7	823.4
Pd/RGO	45.5	53.9	44.2	37.6	526.1	447.3
Pd/CNT	28.6	30.8	40.3	30.9	450.7	345.4
Pd/XC-72	16.8	12.9	10.9	7.7	121.9	85.9

ECSA value calculated for Pd/PG (103.8 m^2/g, CV of PG in 0.5 M H_2SO_4 solution is shown in Figure S6, Supporting Information) is at least twice as high as that obtained for Pd/RGO (45.5 m^2/g), three times Pd/CNT (28.6 m^2/g), and six times Pd/XC-72 (16.8 m^2/g). The ECSA of Pd/PG is also higher than commercial E-TEK catalyst (21.0 m^2/g),[52] Pd/RGO/polypyrrolehybrids (63.6 m^2/g),[53] Pd/graphene (72.7 m^2/g),[54] and those of state of the art Pt-based nanomaterials in acid medium, such as Pt/low-defect graphene (63.0 m^2/g),[48] Pt/GO (16.9 m^2/g),[55] Pt/RGO (44.6 m^2/g),[56] and graphene-based Pt-on-Pd bimetallic nanodendrite catalyst (81.6 m^2/g),[57] Pt/polyaniline (64.5 m^2/g),[13] Pt/CNT (33.4 m^2/g),[58] Pt/CNT/ionic liquid (71.4 m^2/g),[59] that is, the utilization of Pd in Pd/PG is very high.

The electrocatalytic performance of the Pd catalysts was also evaluated in alkaline medium. As displayed in in Figure 5b and Table 1, Pd/PG shows a larger ECSA value (115.0 m^2/g),[60,61] at least twice that of Pd/RGO (53.9 m^2/g) and Pd/CNT (30.8 m^2/g), 8 times that of Pd/XC-72 (12.9 m^2/g), far surpassing recently reported Pd-based nanostructures such as Pd/polypyrrole/RGO (41.8 m^2/g),[19] Pd/MnO_2/MWNT (35.6 m^2/g),[62] Pt–Pd/carbon hybrids (51.4 m^2/g),[63] and Pd/Co_3O_4/XC-72 (48.0 m^2/g),[64] that is, Pd/PG also possesses excellent electrocatalytic activity in alkaline media. These remarkable enhancements are due to not only fine dispersibility of the Pd nanoparticles on the large surface area 2D carbon material but also well-preserved intrinsic electrical conductivity of graphene in Pd/PG.

We tested the composites in electro-oxidation of formic acid and methanol using cyclic voltammetry. Figure 6a depicts the CVs of the electrodes coated with Pd/PG, Pd/RGO, Pd/CNT, and Pd/XC-72, immersed in a 0.5 M HCOOH and 0.5 M H_2SO_4 mixed solution at 50 mV s^{-1}. All curves show obvious

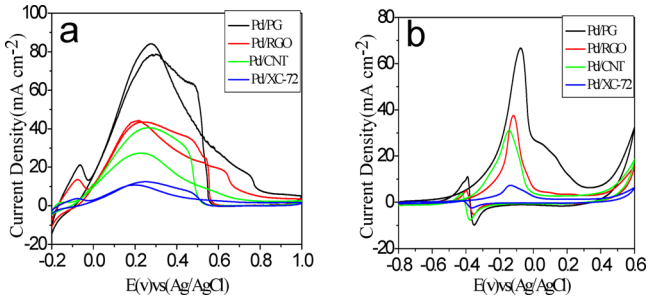

Figure 6. CVs of Pd/PG, Pd/RGO, Pd/CNT, and Pd/XC-72 in (a) 0.5 M H_2SO_4 with 0.5 M HCOOH and (b) 0.5 M NaOH with 1 M methanol at 50 mV s^{-1}.

oxidation peaks and a minor hump at 0.45–0.75 V between the positive potential excursions, which are associated with direct oxidation of formic acid and oxidation of Pd. During the subsequent negative excursion, a broad oxidation peak appeared due to stripping of the absorbed intermediates and regeneration of the Pd surface. As can be seen in Table 1, the Pd/PG catalyst exhibits a considerably high mass activity of 1045.7 mA mg^{-1} Pd as compared with those (526.1, 450.7, and 121.9 mA mg^{-1} Pd) of Pd/RGO, Pd/CNT, and Pd/XC-72 catalysts. In the presence of 0.5 M NaOH and 1.0 M methanol, two methanol oxidation peaks were clearly observed. In this case, the mass activity (823.4 mA mg^{-1} Pd) of Pd/PG is 1.8, 2.4, and 9.6 times that of Pd/RGO, Pd/CNT, and Pd/XC-72 (Figure 6b and Table 1).

For comparison, some reported state-of-art Pd-based nanomaterials are listed in Table S1 and S2, Supporting Information. These results confirm that the synergetic effects of particle dispersion and the intrinsic structure of pristine graphene in the hybrid are essential for promoting the formic acid and methanol oxidation reactions.

It is well known that the stability of catalysts is important for the application of fuel cells.[7] Chronoamperometric (CA) measurement was used to test the durability of catalysts. Figure 7a shows the CA curves of the Pd/PG, Pd/RGO, Pd/

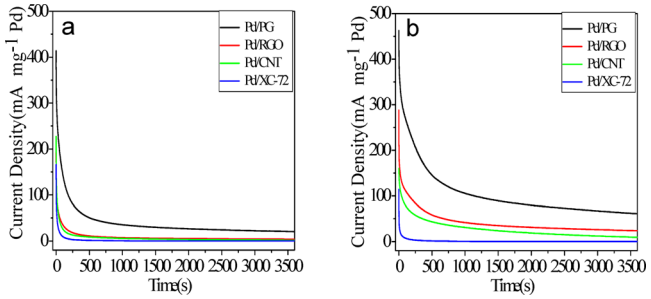

Figure 7. Current–time dependence measured by chronoamperometry in (a) 0.5 M H_2SO_4 with 0.5 M HCOOH at 0.15 V (vs Ag/AgCl) and (b) 0.5 M NaOH with 1 M methanol at 0.2 V (vs Ag/AgCl) for Pd/PG, Pd/RGO, Pd/CNT, and Pd/XC-72.

CNT, and Pd/XC-72 electrodes in a 0.5 M H_2SO_4 and 0.5 M HCOOH solution at a constant potential of 0.15 V. The decay of the current density was found for all catalysts because of the formation of the intermediate carbonaceous species during the formic acid oxidation reaction. The most rapid initial decay was observed for the Vulcan XC-72-based Pd catalysts. For Pd/PG, the decay rate is lower compared to other catalysts in the initial period. During the entire process, the highest current density is

DOI: 10.1021/la5049425
Langmuir 2015, 31, 2576–2583

found in Pd/PG, indicating its optimal performance and stability for formic acid oxidation. The poor stability of the RGO-based composite is due to particle aggregation and uneven distribution on RGO, thus suffering from accumulation of more absorbed surface carbonaceous intermediates. Another possibility is associated with the dense defects on RGO. The RGO-based composite corrodes easily under harsh chemical or electrochemical oxidation conditions. For methanol oxidation, the current decay rate (Figure 7b) exhibits a similar trend in the order Pd/PG < Pd/RGO < Pd/CNT< Pd/XC-72, in line with the CV results. Apart from fine dispersion of the Pd nanoparticles, a few-layer graphene structure is also beneficial to the enhanced stability of Pd/PG. The outmost graphene layer may be easily corroded, but more graphene layers of Pd/PG retain the graphitized base structure.

Electrochemical impedance spectra (EIS) were conducted to assess the electric conductive performance of the composites. Figure 8 shows the Nyquist plots of the Pd/PG, Pd/RGO, Pd/CNT, and Pd/XC-72 composites obtained in a solution of 0.5 M HCOOH and 0.5 M H_2SO_4 at a potential of 0.2 V (vs Ag/AgCl). A partially overlapped semicircle is found in the Nyquist plots of the catalysts. The charge transfer resistance of catalysts can be determined by the diameter of primary semicircle. ZView software was used to fit the impedance data.[65] The charge transfer resistance (R_{ct}) values are 101.4, 173.9, 232.3, and 251.3 Ω for Pd/PG, Pd/RGO, Pd/CNT, and Pd/XC-72, respectively. The charge transfer resistances of graphene-based composites (Pd/PG and Pd/RGO) are considerably smaller than that in Pd/CNT and Pd/XC-72, suggesting superior electrical conductivity of graphene as an electrocatalyst material in comparison with the traditional carbon-supporting substrate. In addition, Pd/PG has a significantly lower R_{ct} value than Pd/RGO. Thus, the highly crystalline nature of graphene is essential for promoting the electron transport. The decrease in the R_{ct} value for the PG-based catalyst is indicative of decreased reaction resistance of formic acid electro-oxidation and well correlated to the improved catalytic activity.

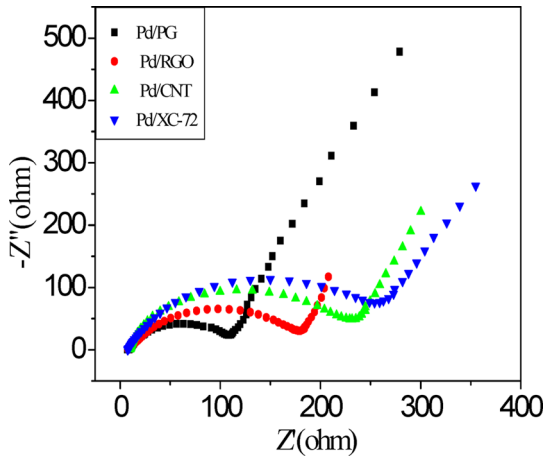

Figure 8. Nyquist plots of EIS for Pd/PG, Pd/RGO, Pd/CNT, and Pd/XC-72 at 0.2 V (vs Ag/AgCl) in 0.5 M H_2SO_4 with 0.5 M HCOOH.

4. CONCLUSIONS

We developed pristine graphene-supported Pd electrocatalysts using a simple supercritical method. The supercritical carbon dioxide was found to uniformly disperse the worm-like Pd nanoparticles that help debundle the graphene nanosheets The resulting Pd/PG nanohybrid exhibits excellent electrocatalytic activity and stability for both formic acid and methanol oxidation reactions, far surpassing the Pd/RGO, Pd/CNT, and Pd/XC-72 hybrids. The superior electrocatalytic property of Pd/PG is attributed to the unique graphitic basal plane structure of pristine graphene that offers large surfaces, high electrical conductivity, and chemical stability. The unique supercritical strategy is practically viable but not constrained to loading of other nanosized metal particles or quantum dots on pristine graphene for different engineering applications and functionality.

■ ASSOCIATED CONTENT

Ⓢ Supporting Information

This material is available free of charge via the Internet at http://pubs.acs.org.

■ AUTHOR INFORMATION

Corresponding Authors

*Phone: +86 0532 84023847. Fax: +86 0532 84022725. E-mail: zhaojian@gmail.com.
*E-mail: zp@tongji.edu.cn.

Notes

The authors declare no competing financial interest.

■ ACKNOWLEDGMENTS

The work was funded by the National Natural Science Foundation of China (nos. 51073082 and 51373088).

■ REFERENCES

(1) Arico, A.; Srinivasan, S.; Antonucci, V. DMFCs: from fundamental aspects to technology development. *Fuel Cells* **2001**, *1* (2), 133−161.
(2) Paik, Y.; Kim, S. S.; Han, O. H. Methanol behavior in direct methanol fuel cells. *Angew. Chem., Int. Ed.* **2008**, *47* (1), 94−96.
(3) Zhang, S.; Shao, Y.; Yin, G.; Lin, Y. Electrostatic Self-Assembly of a Pt-around-Au Nanocomposite with High Activity towards Formic Acid Oxidation. *Angew. Chem., Int. Ed.* **2010**, *49* (12), 2211−2214.
(4) Mazumder, V.; Sun, S. Oleylamine-mediated synthesis of Pd nanoparticles for catalytic formic acid oxidation. *J. Am. Chem. Soc.* **2009**, *131* (13), 4588−4589.
(5) Pandey, R. K.; Lakshminarayanan, V. Electro-oxidation of formic acid, methanol, and ethanol on electrodeposited Pd-polyaniline nanofiber films in acidic and alkaline medium. *J. Phys. Chem.C* **2009**, *113* (52), 21596−21603.
(6) Guo, S.; Dong, S.; Wang, E. Three-Dimensional Pt-on-Pd Bimetallic Nanodendrites Supported on Graphene Nanosheet: Facile Synthesis and Used as an Advanced Nanoelectrocatalyst for Methanol Oxidation. *ACS Nano* **2009**, *4* (1), 547−555.
(7) Yu, X.; Pickup, P. G. Recent advances in direct formic acid fuel cells (DFAFC). *J. Power Sources* **2008**, *182* (1), 124−132.
(8) Chen, X.; Wu, G.; Chen, J.; Chen, X.; Xie, Z.; Wang, X. Synthesis of "clean" and well-dispersive Pd nanoparticles with excellent electrocatalytic property on graphene oxide. *J. Am. Chem. Soc.* **2011**, *133* (11), 3693−3695.
(9) Huang, H.; Wang, X. Recent progress on carbon-based support materials for electrocatalysts of direct methanol fuel cells. *J. Mater. Chem. A* **2014**, *2* (18), 6266−6291.
(10) Feng, L.; Yao, S.; Zhao, X.; Yan, L.; Liu, C.; Xing, W. Electrocatalytic properties of Pd/C catalyst for formic acid electro-oxidation promoted by europium oxide. *J. Power Sources* **2012**, *197*, 38−43.
(11) Huang, J.; Liu, Y.; Hou, H.; You, T. Simultaneous electrochemical determination of dopamine, uric acid and ascorbic acid using

DOI: 10.1021/la5049425
Langmuir 2015, 31, 2576−2583

palladium nanoparticle-loaded carbon nanofibers modified electrode. *Biosens. Bioelectron.* **2008**, *24* (4), 632−637.
(12) Chen, C.; Liou, W.; Lin, H.; Wu, S.; Borodzinski, A.; Stobinski, L.; Kedzierzawski, P. Palladium and palladium gold catalysts supported on MWCNTs for electrooxidation of formic acid. *Fuel Cells* **2010**, *10* (2), 227−233.
(13) He, D.; Zeng, C.; Xu, C.; Cheng, N.; Li, H.; Mu, S.; Pan, M. Polyaniline-functionalized carbon nanotube supported platinum catalysts. *Langmuir* **2011**, *27* (9), 5582−5588.
(14) Li, X.; Zhu, Y.; Cai, W.; Borysiak, M.; Han, B.; Chen, D.; Piner, R. D.; Colombo, L.; Ruoff, R. S. Transfer of large-area graphene films for high-performance transparent conductive electrodes. *Nano Lett.* **2009**, *9* (12), 4359−4363.
(15) Schniepp, H. C.; Li, J.L.; McAllister, M. J.; Sai, H.; Herrera-Alonso, M.; Adamson, D. H.; Prud'homme, R. K.; Car, R.; Saville, D. A.; Aksay, I. A. Functionalized single graphene sheets derived from splitting graphite oxide. *J. Phys. Chem. B* **2006**, *110* (17), 8535−8539.
(16) Bong, S.; Uhm, S.; Kim, Y.R.; Lee, J.; Kim, H. Graphene supported Pd electrocatalysts for formic acid oxidation. *Electrocatalysis* **2010**, *1* (2-3), 139−143.
(17) Yang, J.; Tian, C.; Wang, L.; Fu, H. An effective strategy for small-sized and highly-dispersed palladium nanoparticles supported on graphene with excellent performance for formic acid oxidation. *J. Mater. Chem.* **2011**, *21* (10), 3384−3390.
(18) Jin, T.; Guo, S.; Zuo, J.L.; Sun, S. Synthesis and assembly of Pd nanoparticles on graphene for enhanced electrooxidation of formic acid. *Nanoscale* **2013**, *5* (1), 160−163.
(19) Zhao, Y.; Zhan, L.; Tian, J.; Nie, S.; Ning, Z. Enhanced electrocatalytic oxidation of methanol on Pd/polypyrrole−graphene in alkaline medium. *Electrochim. Acta***2011***56*1967−1972.
(20) Scheuermann, G. M.; Rumi, L.; Steurer, P.; Bannwarth, W.; Mülhaupt, R. Palladium nanoparticles on graphite oxide and its functionalized graphene derivatives as highly active catalysts for the Suzuki− Miyaura coupling reaction. *J. Am. Chem. Soc.* **2009**, *131* (23), 8262−8270.
(21) Wen, Z.; Yang, S.; Liang, Y.; He, W.; Tong, H.; Hao, L.; Zhang, X.; Song, Q. The improved electrocatalytic activity of palladium/graphene nanosheets towards ethanol oxidation by tin oxide. *Electrochim. Acta* **2010**, *56* (1), 139−144.
(22) Yu, Y.; Li, Y.; Pan, Y.; Liu, C.J. Fabrication of palladium/graphene oxide composite by plasma reduction at room temperature. *Nanoscale Res. Lett.* **2012**, *7* (1), 1−4.
(23) Gómez-Navarro, C.; Weitz, R. T.; Bittner, A. M.; Scolari, M.; Mews, A.; Burghard, M.; Kern, K. Electronic transport properties of individual chemically reduced graphene oxide sheets. *Nano Lett.* **2007**, *7* (11), 3499−3503.
(24) Stankovich, S.; Dikin, D. A.; Piner, R. D.; Kohlhaas, K. A.; Kleinhammes, A.; Jia, Y.; Wu, Y.; Nguyen, S. T.; Ruoff, R. S. Synthesis of graphene-based nanosheets via chemical reduction of exfoliated graphite oxide. *Carbon* **2007**, *45* (7), 1558−1565.
(25) Lotya, M.; King, P. J.; Khan, U.; De, S.; Coleman, J. N. High-concentration, surfactant-stabilized graphene dispersions. *ACS Nano* **2010**, *4* (6), 3155−3162.
(26) Song, C.; Wu, D.; Zhang, F.; Liu, P.; Lu, Q.; Feng, X. Gemini surfactant assisted synthesis of two-dimensional metal nanoparticles/graphene composites. *Chem. Commun.* **2012**, *48* (15), 2119−2121.
(27) Kundu, P.; Nethravathi, C.; Deshpande, P. A.; Rajamathi, M.; Madras, G.; Ravishankar, N. Ultrafast microwave-assisted route to surfactant-free ultrafine Pt nanoparticles on graphene: synergistic co-reduction mechanism and high catalytic activity. *Chem. Commun.* **2011**, *23* (11), 2772−2780.
(28) Zhao, J.; Zhang, L.; Chen, T.; Yu, H.; Zhang, L.; Xue, H.; Hu, H. Supercritical Carbon-Dioxide-Assisted Deposition of Pt Nanoparticles on Graphene Sheets and Their Application as an Electrocatalyst for Direct Methanol Fuel Cells. *J. Phys. Chem. C* **2012**, *116* (40), 21374−21381.
(29) Zhao, J.; Zhang, L.; Xue, H.; Wang, Z.; Hu, H. Methanol electrocatalytic oxidation on highly dispersed platinum−ruthenium/graphene catalysts prepared in supercritical carbon dioxide−methanol solution. *RSC Adv.* **2012**, *2* (25), 9651−9659.
(30) Kim, Y.T.; Lee, H.; Kim, H.J.; Lim, T.H. PtRu nano-dandelions on thiolated carbon nanotubes: a new synthetic strategy for supported bimetallic core−shell clusters on the atomic scale. *Chem. Commun.* **2010**, *46* (12), 2085−2087.
(31) Becerril, H. A.; Mao, J.; Liu, Z.; Stoltenberg, R. M.; Bao, Z.; Chen, Y. Evaluation of solution-processed reduced graphene oxide films as transparent conductors. *ACS Nano* **2008**, *2* (3), 463−470.
(32) Hummers, W. S., Jr; Offeman, R. E. Preparation of graphitic oxide. *J. Am. Chem. Soc.* **1958**, *80* (6), 1339−1339.
(33) Khan, U.; Porwal, H.; O'Neill, A.; Nawaz, K.; May, P.; Coleman, J. N. Solvent-exfoliated graphene at extremely high concentration. *Langmuir* **2011**, *27* (15), 9077−9082.
(34) Choi, S. M.; Seo, M. H.; Kim, H. J.; Kim, W. B. Synthesis of surface-functionalized graphene nanosheets with high Pt-loadings and their applications to methanol electrooxidation. *Carbon* **2011**, *49* (3), 904−909.
(35) Maillard, F.; Bonnefont, A.; Chatenet, M.; Guétaz, L.; Doisneau-Cottignies, B.; Roussel, H.; Stimming, U. Effect of the structure of Pt−Ru/C particles on CO_{ad} monolayer vibrational properties and electrooxidation kinetics. *Electrochim. Acta* **2007**, *53* (2), 811−822.
(36) Sun, H.; Jiao, X.; Wang, H.; Jiang, Z.; Chen, D. Solvothermal preparation of Pd nanostructures under nitrogen and air atmospheres and electrocatalytic activities for the oxidation of methanol. *ACS Appl. Mater. Interfaces* **2011**, *3* (7), 2425−2430.
(37) Meyer, J. C.; Geim, A. K.; Katsnelson, M.; Novoselov, K.; Booth, T.; Roth, S. The structure of suspended graphene sheets. *Nature* **2007**, *446* (7131), 60−63.
(38) Hernández-Fernández, P.; Montiel, M.; Ocón, P.; de la Fuente, J.; García-Rodríguez, S.; Rojas, S.; Fierro, J. Functionalization of multi-walled carbon nanotubes and application as supports for electro-catalysts in proton-exchange membrane fuel cell. *Appl. Catal. B: Environ.* **2010**, *99* (1), 343−352.
(39) Ferrari, A.; Meyer, J.; Scardaci, V.; Casiraghi, C.; Lazzeri, M.; Mauri, F.; Piscanec, S.; Jiang, D.; Novoselov, K.; Roth, S. Raman spectrum of graphene and graphene layers. *Phys. Rev. Lett.* **2006**, *97* (18), 187401.
(40) Wang, Y. Y.; Ni, Z. H.; Yu, T.; Shen, Z. X.; Wang, H. M.; Wu, Y. H.; Chen, W.; Shen Wee, A. T. Raman studies of monolayer graphene: the substrate effect. *Phys. Rev. Lett.C* **2008**, *112* (29), 10637−10640.
(41) Ferrari, A. C. Raman spectroscopy of graphene and graphite: disorder, electron−phonon coupling, doping and nonadiabatic effects. *Solid State Commun.* **2007**, *143* (1), 47−57.
(42) O'Neill, A.; Khan, U.; Nirmalraj, P. N.; Boland, J.; Coleman, J. N. Graphene dispersion and exfoliation in low boiling point solvents. *Phys. Rev. Lett. C* **2011**, *115* (13), 5422−5428.
(43) Calizo, I.; Balandin, A.; Bao, W.; Miao, F.; Lau, C. Temperature dependence of the Raman spectra of graphene and graphene multilayers. *Nano Lett.* **2007**, *7* (9), 2645−2649.
(44) Kudin, K. N.; Ozbas, B.; Schniepp, H. C.; Prud'Homme, R. K.; Aksay, I. A.; Car, R. Raman spectra of graphite oxide and functionalized graphene sheets. *Nano Lett.* **2008**, *8* (1), 36−41.
(45) Dreyer, D. R.; Park, S.; Bielawski, C. W.; Ruoff, R. S. The chemistry of graphene oxide. *Chem. Soc. Rev.* **2010**, *39* (1), 228−240.
(46) Chen, W.; Yan, L.; Bangal, P. Chemical reduction of graphene oxide to graphene by sulfur-containing compounds. *J. Phys. Chem. C* **2010**, *114* (47), 19885−19890.
(47) Tuinstra, F.; Koenig, J. Characterization of graphite fiber surfaces with Raman spectroscopy. *J. Compos. Mater.* **1970**, *4* (4), 492−499.
(48) Huang, H.; Chen, H.; Sun, D.; Wang, X. Graphene nanoplate-Pt composite as a high performance electrocatalyst for direct methanol fuel cells. *J. Power Sources* **2012**, *204*, 46−52.
(49) Shafiei, M.; Spizzirri, P. G.; Arsat, R.; Yu, J.; du Plessis, J.; Dubin, S.; Kaner, R. B.; Kalantar-Zadeh, K.; Wlodarski, W. Platinum/graphene nanosheet/SiC contacts and their application for hydrogen gas sensing. *J. Phys. Chem.C* **2010**, *114* (32), 13796−13801.

DOI: 10.1021/la5049425
Langmuir 2015, 31, 2576−2583

(50) Halder, A.; Sharma, S.; Hegde, M.; Ravishankar, N. Controlled attachment of ultrafine platinum nanoparticles on functionalized carbon nanotubes with high electrocatalytic activity for methanol oxidation. *J. Phys. Chem. C* **2009**, *113* (4), 1466−1473.
(51) Li, Y.; Fan, X.; Qi, J.; Ji, J.; Wang, S.; Zhang, G.; Zhang, F. Palladium nanoparticle-graphene hybrids as active catalysts for the Suzuki reaction. *Nano Res.* **2010**, *3* (6), 429−437.
(52) Maiyalagan, T.; Nassr, A. B. A.; Alaje, T.; Bron, M.; Scott, K. Three-dimensional cubic ordered mesoporous carbon (CMK-8) as highly efficient stable Pd electro-catalyst support for formic acid oxidation. *J. Power Sources* **2012**, *211*, 147−153.
(53) Yang, S.; Shen, C.; Liang, Y.; Tong, H.; He, W.; Shi, X.; Zhang, X.; Gao, H.J. Graphene nanosheets-polypyrrole hybrid material as a highly active catalyst support for formic acid electro-oxidation. *Nanoscale* **2011**, *3* (8), 3277−3284.
(54) Zhao, H.; Yang, J.; Wang, L.; Tian, C.; Jiang, B.; Fu, H. Fabrication of a palladium nanoparticle/graphene nanosheet hybrid via sacrifice of a copper template and its application in catalytic oxidation of formic acid. *Chem. Commun.* **2011**, *47* (7), 2014−2016.
(55) Seger, B.; Kamat, P. V. Electrocatalytically active graphene-platinum nanocomposites. Role of 2-D carbon support in PEM fuel cells. *J. Phys. Chem. C* **2009**, *113* (19), 7990−7995.
(56) Li, Y.; Tang, L.; Li, J. Preparation and electrochemical performance for methanol oxidation of pt/graphene nanocomposites. *Electron. Commun.* **2009**, *11* (4), 846−849.
(57) Guo, S.; Wen, D.; Zhai, Y.; Dong, S.; Wang, E. Platinum nanoparticle ensemble-on-graphene hybrid nanosheet: one-pot, rapid synthesis, and used as new electrode material for electrochemical sensing. *ACS Nano* **2010**, *4* (7), 3959−3968.
(58) Li, Y.; Gao, W.; Ci, L.; Wang, C.; Ajayan, P. M. Catalytic performance of Pt nanoparticles on reduced graphene oxide for methanol electro-oxidation. *Carbon* **2010**, *48* (4), 1124−1130.
(59) Wu, B.; Hu, D.; Kuang, Y.; Liu, B.; Zhang, X.; Chen, J. Functionalization of Carbon Nanotubes by an Ionic-Liquid Polymer: Dispersion of Pt and PtRu Nanoparticles on Carbon Nanotubes and Their Electrocatalytic Oxidation of Methanol. *Angew. Chem., Int. Ed.* **2009**, *48* (26), 4751−4754.
(60) Kakati, N.; Maiti, J.; Lee, S.; Yoon, Y. Core shell like behavior of PdMo nanoparticles on multiwall carbon nanotubes and their methanol oxidation activity in alkaline medium. *Int. J. Hydrogen Energy* **2012**, *37* (24), 19055−19064.
(61) Huang, H.; Wang, X. Design and synthesis of Pd−MnO 2 nanolamella−graphene composite as a high-performance multifunctional electrocatalyst towards formic acid and methanol oxidation. *Phys. Chem. Chem. Phys.* **2013**, *15* (25), 10367−10375.
(62) Zhao, Y.; Zhan, L.; Tian, J.; Nie, S.; Ning, Z. MnO_2 modified multi-walled carbon nanotubes supported Pd nanoparticles for methanol electro-oxidation in alkaline media. *Int. J. Hydrogen Energy* **2010**, *35* (19), 10522−10526.
(63) Mahapatra, S.; Dutta, A.; Datta, J. Temperature dependence on methanol oxidation and product formation on Pt and Pd modified Pt electrodes in alkaline medium. *Int. J. Hydrogen Energy* **2011**, *36* (22), 14873−14883.
(64) Xu, C.; Tian, Z.; Shen, P.; Jiang, S. P. Oxide (CeO2, NiO, Co3O4 and Mn3O4)-promoted Pd/C electrocatalysts for alcohol electrooxidation in alkaline media. *Electrochim. Acta* **2008**, *53* (5), 2610−2618.
(65) Wang, Z.B.; Yin, G.P.; Shao, Y.Y.; Yang, B.Q.; Shi, P.F.; Feng, P.X. Electrochemical impedance studies on carbon supported PtRuNi and PtRu anode catalysts in acid medium for direct methanol fuel cell. *J. Power Sources* **2007**, *165* (1), 9−15.

DOI: 10.1021/la5049425
Langmuir 2015, 31, 2576−2583